Journal of Turbulence
Vol. 14, No. 7, 49-70, 2013, 1–25

PUBLISHED PAPER

Effective eddy viscosity in stratified turbulence

Sina Khani[a*] and Michael L. Waite[a]

[a]*Department of Applied Mathematics, University of Waterloo, 200 University Avenue West, Waterloo, Ontario N2L 3G1, Canada*

(*15 August 2013*)

This paper investigates the effective eddy viscosity inferred from direct numerical simulations of decaying stratified and non-stratified turbulence. It is shown that stratification affects the horizontal eddy viscosity dramatically, by increasing non-local energy transfer between large and small horizontal scales. This non-local horizontal energy transfer is around 20% of the local horizontal energy transfer at the cutoff wavenumber $k_c = 40$. The non-local horizontal energy transfer occurs at large vertical wavenumbers, which may be larger than the buoyancy wavenumber $k_b = N/u_{rms}$, where N is the buoyancy frequency and u_{rms} is the root-mean-square velocity. By increasing the value of the test cutoff wavenumber k_c from large scales to the dissipation range, the non-local horizontal eddy viscosity decreases and the local eddy viscosity is dominant. Overall, the presence of stratification can significantly change the features of subgrid-scale (SGS) motions. Current SGS models should therefore be modified for use in large-eddy simulation of stratified turbulence.

Keywords: stratified turbulence; direct numerical simulation; effective eddy viscosity

1. Introduction

The nature of turbulence in the atmosphere and the ocean is characterized by very high Reynolds numbers. Moreover, in the atmospheric mesosphere and the oceanic sub-mesoscale range, turbulent flows are strongly affected by stable stratification, but only weakly affected by the Earth's rotation [1]. Thus, vertical motions are restrained by buoyancy forces and horizontal structures are elongated into anisotropic pancake-like vortices [2, 3]. Such flows can have Reynolds numbers of the order 10^8 or higher. Performing a direct numerical simulation (DNS) at such scales, therefore, requires that an enormous range of scales be resolved. Such resolution is not possible because of high computational memory and time costs. Large-eddy simulation (LES) is an alternative approach that removes the need to resolve any but the large-scale motions. The basic idea behind LES is to explicitly resolve large scales and to model the effects of small scales on large ones through subgrid-scale (SGS) models.

Recent advances in the understanding of geophysical turbulence have described the appearance of stratified turbulence when the buoyancy Reynolds number is sufficiently high and the horizontal Froude number is sufficiently low [4–7]. Under such conditions, the inertial subrange of stratified turbulence is divided into an anisotropic range at large scales and an isotropic range at small scales. The anisotropic and isotropic parts of the inertial subrange are separated by the Ozmidov [8] wavenumber $k_o = (N^3/\epsilon)^{1/2}$, where ϵ is the kinetic energy dissipation rate

*Corresponding author. Email: sinakhani@uwaterloo.ca

ISSN: 1468-5248 (online only)

DOI: 10.1080/14685248.2013.837913
http://www.tandfonline.com

and N is the buoyancy frequency. Generally, SGS models are used to model small-scale isotropic turbulence [9–13]. In the inertial subrange of isotopic turbulence, the energy spectrum $E(k)$ is [14]:

$$E(k) \sim \epsilon^{2/3} k^{-5/3}, \tag{1}$$

where $k = \sqrt{k_x^2 + k_y^2 + k_z^2}$ is the total wavenumber. However, stratified turbulence includes an additional anisotropic subrange because of stratification. According to the stratified turbulence hypothesis [5, 6], the energy spectrum in this range is proportional to different power laws in the horizontal and vertical wavenumbers:

$$E(k_h) \sim \epsilon^{2/3} k_h^{-5/3} \qquad\qquad E(k_v) \sim N^2 k_v^{-3}, \tag{2}$$

where $k_h = \sqrt{k_x^2 + k_y^2}$ and $k_v = |k_z|$ respectively stand for the wavenumbers in the horizontal and vertical directions. Although simulations are largely consistent with these predictions, the universality of $-5/3$ and -3 slopes is still under investigation [6, 15–18]. Isotropic SGS models do not seem to be the proper approach for modelling the effects of turbulent scales in the anisotropic part of the stratified turbulence inertial range. Since these models have been designed to represent the effects of small-scale motions in the isotropic subrange, it is important to study in detail the features of the anisotropic inertial subrange. One approach is to directly measure the effective spectral eddy viscosity using DNS results. This type of fundamental analysis has already been done for the Kolmogorov isotropic inertial subrange (as in e.g. Domaradzki et al. [19, 20]), but it is not been studied so far for the anisotropic stratified turbulence. The main aim of this paper is to study the dynamics of energy transfer in the anisotropic inertial subrange of stratified turbulence using the effective eddy viscosity point of view. A theoretical spectral eddy viscosity model for isotropic turbulence has been suggested by Kraichnan [10], who considered an infinite inertial subrange. The Kraichnan eddy viscosity model includes two parts: a constant plateau at small wavenumbers, which represents the non-local energy transfer between SGS motions and large resolved scales, and a cusp near the cutoff wavenumber k_c, which accounts for the local energy transfer around the cutoff [10, 21].

In this paper, we use DNS of stratified turbulence to explicitly measure the effective spectral eddy viscosity in the horizontal and vertical directions, following Lindborg's [5] hypothesis of an anisotropic cascade from large to small horizontal scales. If the cascade to small scales is fundamentally anisotropic, the shapes of the effective eddy viscosity in the horizontal and vertical directions will provide insight into the nature of this energy transfer. We compare the results of this study to those of the original Kraichnan eddy viscosity model [10] and also Domaradzki's [19, 20] results for unstratified turbulence, and evaluate how different they are. Our objective is to clarify the effects of stratification on SGS models. In Section 2 we review the literature on stratified flows and DNS and LES of stratified turbulence. This section also describes the governing equations of stratified flows as well as equations for measuring effective eddy viscosity. An overview of our numerical experiments and initial conditions is presented in Section 3. In Section 4, we present our simulation results and discuss the effects of stratification, Reynolds numbers, and the cutoff location. Finally, conclusions are given in Section 5.

2. Background

Strong stratification generates horizontal motions with large vertical shear, referred to as layered pancake structures [3, 22, 23]. Although Gage [22] and Lilly [23] proposed an inverse energy cascade (in analogy with two-dimensional turbulence) for these anisotropic three-dimensional structures, more recent results point to a downscale cascade (e.g. Lindborg [5]). The vertical scale [3, 15] of the pancake structures is u_{rms}/N, which yields a vertical Froude number of $O(1)$. This scaling for the vertical Froude number is the basis for the stratified turbulence hypothesis [5, 6] in which the inertial subrange has an anisotropic part at large scales in addition to the classical isotropic part at small scales.

Several studies have investigated numerical simulations of stratified turbulence, both DNS [4, 6, 17, 18] and LES [12, 24–26]. The main disadvantage of the DNS approach is its intrinsic limitation in achieving high Reynolds number flows. For example, in the DNS study by Almalkie and de Bruyn Kops [17], in which the spatial resolution is very high, the maximum Reynolds number is $O(10^4)$. On the other hand, the LES of Siegel and Domaradzki [12] and Carnevale et al. [25], who used spatial and spectral eddy viscosity, respectively, neglected the effects of anisotropy in their SGS models. In addition, the implicit LES (ILES) approach (e.g. Remmeler and Hickel [26]) uses numerical diffusion to represent SGS, and thus very sensitive to the numerical scheme [27]. Therefore, there is a real need for better understanding of SGS motions of stratified flows.

The non-dimensionalized Navier-Stokes equations under the Boussinesq approximation are

$$\frac{\partial \boldsymbol{u}}{\partial t} + \boldsymbol{u}\cdot\nabla\boldsymbol{u} = -\nabla p - \frac{1}{{Fr_\ell}^2}\rho\boldsymbol{e}_z + \frac{1}{Re_\ell}\nabla^2\boldsymbol{u}, \tag{3}$$

$$\nabla\cdot\boldsymbol{u} = 0, \tag{4}$$

$$\frac{\partial \rho}{\partial t} + \boldsymbol{u}\cdot\nabla\rho - w = \frac{1}{Re_\ell Pr}\nabla^2\rho, \tag{5}$$

where $\boldsymbol{u}$ is the velocity vector, and ρ and p are the density and pressure fluctuations from their ambient values. The initial Reynolds number Re_ℓ, Froude number Fr_ℓ, and Prandtl number Pr are defined as

$$Re_\ell = \frac{u\ell}{\nu}, \tag{6}$$

$$Fr_\ell = \frac{u}{N\ell}, \tag{7}$$

$$Pr = \frac{\nu}{D}, \tag{8}$$

where u and ℓ are the initial velocity- and length-scales, respectively, ν is the molecular viscosity, and D is the mass diffusivity. In this work, we take $Pr = 1$ and assume constant N. This latter assumption is common in idealized studies of stratified turbulence [4, 6, 7, 15, 16, 18].

Assuming periodic boundary conditions, a flow variable $f(\boldsymbol{x}, t)$ can be expanded in a Fourier series as

$$f(\boldsymbol{x},t) = \sum_{\boldsymbol{k}} \hat{f}(\boldsymbol{k},t) e^{i\boldsymbol{k}\cdot\boldsymbol{x}}, \tag{9}$$

where $\hat{f}(\boldsymbol{k},t)$ is the Fourier coefficient of f, and the sum is up to an isotropic cutoff $|\boldsymbol{k}| < k_{max}$. In DNS, k_{max} is set to be around the Kolmogorov wavenumber

$$k_d = (\frac{\epsilon}{\nu^3})^{\frac{1}{4}}, \tag{10}$$

which ensures that the dissipation is resolved. Our k_{max}/k_d is always greater than 0.5, which, following Moin and Mahesh [28], means that most of the dissipation is resolved. The equations of motion (3-5) can be re-written as

$$(\frac{\partial}{\partial t} + \frac{k^2}{Re_\ell})\hat{u}_j(\boldsymbol{k},t) + \frac{1}{{Fr_\ell}^2}\hat{\rho}(\boldsymbol{k},t)\boldsymbol{e}_z = -ik_m P_{jr}(\boldsymbol{k}) \sum_{\boldsymbol{p}+\boldsymbol{q}=\boldsymbol{k}} \hat{u}_r(\boldsymbol{p},t)\hat{u}_m(\boldsymbol{q},t), \tag{11}$$

$$k_i\hat{u}_i(\boldsymbol{k},t) = 0, \tag{12}$$

$$(\frac{\partial}{\partial t} + \frac{k^2}{Re_\ell Pr})\hat{\rho}(\boldsymbol{k},t) - \hat{w}(\boldsymbol{k},t) = -ik_m \sum_{\boldsymbol{p}+\boldsymbol{q}=\boldsymbol{k}} \hat{u}_m(\boldsymbol{p},t)\hat{\rho}(\boldsymbol{q},t), \tag{13}$$

where the projection tensor $P_{ij}(\boldsymbol{k}) = \delta_{ij} - k_i k_j/k^2$ is used to eliminate the pressure term [29]. If we define a test cutoff wavenumber k_c, we can express the interactions between wavevectors with $|\boldsymbol{k}| > k_c$ and those with $|\boldsymbol{k}| \leq k_c$. Consider the non-linear terms on the right-hand side of equations (11) and (13):

$$F_j(\boldsymbol{k},t) = -ik_m P_{jr}(\boldsymbol{k}) \sum_{\boldsymbol{p}+\boldsymbol{q}=\boldsymbol{k}} \hat{u}_r(\boldsymbol{p},t)\hat{u}_m(\boldsymbol{q},t), \tag{14}$$

$$J(\boldsymbol{k},t) = -ik_m \sum_{\boldsymbol{p}+\boldsymbol{q}=\boldsymbol{k}} \hat{u}_m(\boldsymbol{p},t)\hat{\rho}(\boldsymbol{q},t). \tag{15}$$

The corresponding nonlinear terms in the kinetic and potential energy equations, T_k and T_p, can be obtained by multiplying equations (14) and (15) by $\hat{u}_j^*$ and $(1/{Fr_\ell}^2)\hat{\rho}^*$, and adding the complex conjugates (denoted by $*$) yielding [5, 29, 30]:

$$T_k(\boldsymbol{k},t) = -\frac{i}{2}k_m P_{jr} \sum_{\boldsymbol{p}+\boldsymbol{q}=\boldsymbol{k}} \{\ \hat{u}_j^*(\boldsymbol{k},t)\hat{u}_r(\boldsymbol{p},t)\hat{u}_m(\boldsymbol{q},t) + \hat{u}_j(\boldsymbol{k},t)\hat{u}_r^*(\boldsymbol{p},t)\hat{u}_m^*(\boldsymbol{q},t)\}, \tag{16}$$

$$T_p(\boldsymbol{k},t) = -\frac{i}{2{Fr_\ell}^2}k_m \sum_{\boldsymbol{p}+\boldsymbol{q}=\boldsymbol{k}} \{\ \hat{\rho}^*(\boldsymbol{k},t)\hat{u}_m(\boldsymbol{p},t)\hat{\rho}(\boldsymbol{q},t) + \hat{\rho}(\boldsymbol{k},t)\hat{u}_m^*(\boldsymbol{p},t)\hat{\rho}^*(\boldsymbol{q},t)\}. \tag{17}$$

Based on the cutoff k_c, we can decompose T_k and T_p into $\overline{T_k}$ and $\overline{T_p}$, in which the sums in equations (16) and (17) are restricted to $\boldsymbol{p}$ and $\boldsymbol{q}$ with $|\boldsymbol{p}|$, $|\boldsymbol{q}| < k_c$; and T_k^s and T_p^s, in which at least one of $|\boldsymbol{p}|$ or $|\boldsymbol{q}|$ is above the cutoff k_c. The quantities T_k^s and T_p^s represent energy transfer into $\boldsymbol{k}$ from interactions with wavenumbers above k_c. The spectral eddy viscosity approach models T_k^s and T_p^s by [10, 19, 21, 30]

$$T_k^s(\boldsymbol{k},t) = -2\nu_e(\boldsymbol{k},t)k^2E(\boldsymbol{k},t), \tag{18}$$

$$T_p^s(\boldsymbol{k},t) = \frac{T_k^s(\boldsymbol{k},t)}{Pr_t} = -2\frac{\nu_e(\boldsymbol{k},t)}{Pr_t}k^2E(\boldsymbol{k},t), \tag{19}$$

where $\nu_e(\boldsymbol{k},t)$ is the spectral eddy viscosity coefficient, $E(\boldsymbol{k},t) = \frac{1}{2}\hat{u}_j(\boldsymbol{k},t)\hat{u}_j^*(\boldsymbol{k},t)$ is the kinetic energy in wavevector $\boldsymbol{k}$, and Pr_t is the turbulent Prandtl number (usually assumed to be constant [12, 31, 32]). The eddy viscosity at wavenumber $\boldsymbol{k}$ can therefore be defined as

$$\nu_e(\boldsymbol{k},t) = -\frac{T_k^s(\boldsymbol{k},t)}{2k^2E(\boldsymbol{k},t)}. \tag{20}$$

Assuming an isotropic eddy viscosity, $T_k^s(\boldsymbol{k},t)$ and $E(\boldsymbol{k},t)$ in (20) can be integrated over spheres of radius k to get the spherical eddy viscosity (following the Pope [30] notation) as [19]

$$\nu_e(k|k_c,t) = -\frac{T_k^s(k,t)}{2k^2E(k,t)}, \tag{21}$$

where $T_k^s(k,t)$ is the integrated energy transfer between the cutoff-resolved motions and modes with $k > k_c$, and $E(k,t)$ is the integrated energy spectrum. Here, cutoff-resolved refers to scales with wavenumbers below the test cutoff k_c. This approach was introduced by Domaradzki et al. [19] for measuring effective eddy viscosity in DNS of isotropic turbulence. More recently, Domaradzki & Radhakrishnan [27] measured the effective eddy viscosity in an implicit model of decaying turbulence. They found that without careful choice of the numerical scheme, ILES was unlikely to successfully represent SGS features.

Based on the Lindborg [5] stratified turbulence hypothesis, in which there is an anisotropic cascade from large to small horizontal scales, it seems appropriate to modify the above approach to apply a test cutoff k_c in the horizontal direction. In this case, $T_k^s(\boldsymbol{k},t)$ in (20) changes to $T_k^{s,h}(\boldsymbol{k},t)$, which refers to the energy transfer between modes with $k_h < k_c$, i.e. horizontal cutoff-resolved, and modes with $k_h > k_c$. In this situation, we assume axisymmetric horizontal eddy viscosity, and integrate $T_k^{s,h}(\boldsymbol{k},t)$ and $E(\boldsymbol{k},t)$ over shells of constants k_h to find the horizontal eddy viscosity. In addition, we can also apply the test cutoff k_c in the vertical direction to define $T_k^{s,v}(\boldsymbol{k},t)$ and integrate over k_x and k_y to compute a vertical eddy viscosity. In summary, to measure the horizontal and vertical eddy viscosity, equation (21) can be used if altered somewhat:

$$\nu_e^h(k_h|k_c,t) = -\frac{T_k^{s,h}(k_h,t)}{2k_h^2 E(k_h,t)}, \tag{22}$$

$$\nu_e^v(k_v|k_c,t) = -\frac{T_k^{s,v}(k_v,t)}{2k_v^2 E(k_v,t)}. \tag{23}$$

where $T_k^{s,h}(k_h,t)$ and $T_k^{s,v}(k_v,t)$ are the integrated energy transfer between cutoff-resolved motions and modes with $k_h > k_c$ and $k_v > k_c$, respectively; where k_c is applied accordingly in the horizontal and vertical directions. Moreover, $E(k_h,t)$ and $E(k_v,t)$ are the integrated energy spectrum in the horizontal and vertical directions, respectively.

The distinctions between the horizontal, vertical, and spherical eddy viscosities are important. These eddy viscosities are categorized based on directions in which the test cutoff is applied. When we apply the cutoff k_c in the horizontal direction, for example, we filter at the horizontal cutoff-resolved resolution π/k_c. However, the vertical resolution remains unchanged (i.e. $\Delta z \sim \pi/k_d$). Therefore, by applying the test cutoff k_c in a specific direction, the effective resolution in that direction decreases. As a result, we have a specific eddy viscosity based on the definition of the cutoff k_c in a specific direction. In summary, the kinetic energy equation is affected by these three definitions of the test cutoff k_c in the spherical, horizontal, and vertical directions and are, respectively

$$\frac{\partial E(k,t)}{\partial t} + B(k,t) = \overline{T_k}(k,t) - 2\nu_e(k|k_c,t)k^2 E(k,t), \tag{24}$$

$$\frac{\partial E(k_h,t)}{\partial t} + B(k_h,t) = \overline{T_k}^h(k_h,t) - 2\nu_e^h(k_h|k_c,t)k_h^2 E(k_h,t), \tag{25}$$

$$\frac{\partial E(k_v,t)}{\partial t} + B(k_v,t) = \overline{T_k}^v(k_v,t) - 2\nu_e^v(k_v|k_c,t)k_v^2 E(k_v,t), \tag{26}$$

where the molecular dissipation is neglected for clarity, and

$$B(\boldsymbol{k},t) = \frac{1}{2Fr_\ell^2}\{\hat{\rho}(\boldsymbol{k},t)\hat{w}^*(\boldsymbol{k},t) + \hat{\rho}^*(\boldsymbol{k},t)\hat{w}(\boldsymbol{k},t)\}, \tag{27}$$

is the buoyancy flux, the spherical, horizontal, and vertical wavenumber spectra of which are defined as above.

Applying the test cutoff k_c in different directions (i.e. the horizontal, vertical, and spherical) results in different influences over the triad interactions of $\boldsymbol{p}$, $\boldsymbol{q}$, and $\boldsymbol{k}$ in (16-17). For example, compare the effect of defining the test cutoff in the horizontal direction to that in the spherical one. Applying the cutoff in the horizontal direction, modes with $k_h < k_c$ are retained, but there is no restriction on k_v or k. However, if we apply the cutoff k_c in the spherical direction, all large-scale modes with $k < k_c$ are included; this restriction involves both the horizontal and vertical scales. Hence if, for example, there is an energy exchange between large and small horizontal scales at large vertical wavenumbers, the horizontal eddy viscosity will measure this energy transfer but the spherical eddy viscosity will not. In this case, there is a non-local energy transfer in the horizontal direction, which occurs at large vertical wavenumbers. This energy transfer will therefore lead to a non-local horizontal eddy viscosity but no spherical eddy viscosity. This behaviour could lead to confusion for unstratified turbulence where the underlying cascade

is isotropic. However, given the overwhelming evidence for an anisotropic cascade in stratified turbulence (e.g. [4–6, 15, 33]), the separate consideration of horizontal and vertical eddy viscosity is meaningful and important.

Stratification is characterized in our simulations by two Froude numbers: the initial Froude number, as defined in (7); and a time-dependent horizontal Froude number

$$Fr_h = \frac{u_{rms}}{NL_h}, \tag{28}$$

where u_{rms} is the root-mean-square velocity and the horizontal scale $L_h \equiv [u_{rms}]^3/\epsilon$ is defined using the Taylor hypothesis [6]. We will evaluate this approximation below in Section 4. In the same manner, we define the buoyancy Reynolds number [6] as

$$Re_b = \frac{\epsilon}{\nu N^2}. \tag{29}$$

When the horizontal Froude number Fr_h is sufficiently small (i.e. when flows are strongly stratified), the buoyancy Reynolds number plays a similar role to the Reynolds number in non-stratified flows. In fact, the buoyancy Reynolds number sets the magnitude of the vertical viscous term in the Boussinesq equations [6]. Thus, a flow with a smaller horizontal Froude number (stronger stratification) needs larger Reynolds numbers to ensure turbulence. There are a variety of other Froude numbers defined in the literature; e.g. Riley and de Bruyn Kops [4] used the periodic buoyancy frequency to define the Froude number $2\pi u/N\ell$ which differs from (7) by a factor 2π; the associated buoyancy Reynolds number differs by a significant factor $(2\pi)^2$.

3. Methodology

In this work, DNS of stratified turbulence are employed to measure the effective eddy viscosity. An idealized decaying stratified turbulence test case has been considered, following the DNS of Riley & de Bruyn Kops [4]. The initial condition consists of Taylor-Green (TG) vortices in a periodic cubic domain of size $L = 4\pi$, i.e. two TG wavelengths. The TG vortices are designed to have horizontal structures with vertical variations:

$$\boldsymbol{u}(\boldsymbol{x}, 0) = cos(z)[cos(x)sin(y), -sin(x)cos(y), 0]. \tag{30}$$

Low-level noise of approximately 10% of the initial energy is also added to the initial condition [4]. In our study, the random noise is distributed isotropically, and noise is restricted to wavenumbers with $k_h \leq 7/2$ and $|k_z| \leq 7/2$. Since the non-dimensional domain is 4π, wavenumbers spacing is $1/2$.

The spectral transform method has been used to solve the governing equation with n grid points in the x, y, and z directions. To eliminate aliasing errors, the two-thirds rule [34] with spherical wavenumber truncation is applied, yielding an effective grid spacing of $\Delta x = 1.5L/n$. The third-order Adams-Bashforth scheme is adopted for time-stepping of the nonlinear and buoyancy terms; the implicit

trapezoidal method is used for the diffusion terms. Simulations with two different initial Reynolds numbers $Re_\ell = 6400$ and 800, and three initial Froude numbers $Fr_\ell = 0.32$, 0.64, and ∞ are considered. Finally, four values of $k_c = 10$, 20, 40, 80 are employed as test cutoffs to analyze the effective eddy viscosity. Table 1 shows a list of the parameters and corresponding identifiers used in this study.

4. Results and Discussion

4.1. *Overview of simulations*

Figure 1 illustrates the general evolution of the energy, dissipation rates, kinetic energy spectra, and kinetic energy dissipation spectra for two stratified and one non-stratified cases with the same initial $Re_\ell = 6400$, and one stratified case with initial $Re_\ell = 800$. Figure 1a shows total (kinetic plus potential) energy versus time. The non-stratified case is much less energetic than the stratified case for $t \gtrsim 10$. This behaviour is also evident in Figure 1b, where the total dissipation rate is much higher in the non-stratified turbulence at early time (as in e.g. Remmler & Hickel [26] and Domaradzki et al. [20]). Figures 1c,d show respectively the spherical energy spectrum $E(k)$ and the kinetic energy dissipation spectrum $D(k) = 2\nu k^2 E(k)$ averaged over a time range around the maximum dissipation rates of the stratified and non-stratified cases ($15 \leq t \leq 20$ for the stratified cases with $Fr_\ell = 0.64$; $20 \leq t \leq 25$ for the stratified case with $Fr_\ell = 0.32$; and $10 \leq t \leq 15$ for the non-stratified case). Table 1 shows the range of k_{max}/k_d for all simulations. Since we are interested in results with large Reynolds and buoyancy Reynolds numbers, time averages are computed around the time of maximum ϵ. At these times, the Kolmogorov scale is smallest and hence closest to the grid scale, and k_{max}/k_d reaches the minimum value shown in Table 1, which is still consistent with DNS [28]. This resolution of the Kolmogorov scale is similar to other recent DNS studies of stratified turbulence (e.g. [4, 33, 35, 36]). It is also noteworthy that the large-scale energy increases with decreasing initial Froude number (from $Fr_\ell = \infty$ to 0.64 to 0.32), regardless of the value of the initial Reynolds number (Figures 1c,d).

For the non-stratified case, the approximate time for the onset of turbulence is $t \approx 10$, when the dissipation rate is maximum. However, the time of maximum $\epsilon_{tot} = \epsilon + \epsilon_p$, where ϵ_p is the potential energy dissipation, is postponed in the stratified flows. This behaviour can also be seen in Figure 1a where the total energy is almost constant for $Fr_\ell = 0.64$ up to $t \approx 15$, and for $Fr_\ell = 0.32$ up to $t \approx 20$. Decreasing the initial Froude number from 0.64 to 0.32, at fixed Re_ℓ, may suppress the onset of turbulence as it causes Re_b to fall to around 1 (see below). Hence, in the stratified case, higher Reynolds numbers may be necessary to accelerate the onset of turbulence as in the non-stratified case. The maximum ϵ_{tot} occurs at $t = 15$ for $Fr_\ell = 0.64$ and $t = 21$ for $Fr_\ell = 0.32$. This behaviour demonstrates a delay in the commencement of turbulence caused by decreasing the initial Froude number [4, 35] (and hence the horizontal Froude number as well). The vertical arrows in Figures 1c,d indicate values of the test cutoff k_c, which will be addressed in Section 4.2.

Figure 2 shows the time series of the horizontal Froude number and the buoyancy Reynolds number for two different initial Froude numbers. Recall that the time-dependent L_h is defined using Taylor's hypothesis, which is not expected to be valid when the flow is not turbulent. As a result, Figure 2 does not necessarily yield reasonable results before the commencement of turbulence. Therefore, for $Fr_\ell = 0.64$, Figure 2 is expected to be valid when $t \gtrsim 15$. Similarly, for $Fr_\ell = 0.32$, it is valid when $t \gtrsim 20$. As seen in Figure 2a, the horizontal Froude numbers

are relatively small and fairly close to the Lindborg [5] threshold of value 0.02 for stratified turbulence. (Since Riley & de Bruyn Kops [4] defined their Froude numbers based on the periodic buoyancy frequency, the Froude numbers in Figure 2a should be multiplied by 2π to compare their results [4].) Figure 2b shows that the values of the buoyancy Reynolds number are $O(1)$ for $Fr_\ell = 0.32$ and $O(10)$ for $Fr_\ell = 0.64$, suggesting that these flows are (marginally) strongly stratified turbulence. For case $Fr_\ell = 0.32$, the buoyancy Reynolds number is $Re_b \leq 4$, and so the vertical viscous shear may be significant [6]. In the literature, simulations with $Fr_\ell = 0.64$ and $Fr_\ell = 0.32$, and $Re_\ell = 6400$ have been reported to be inside the strongly stratified turbulence regime [6, 35].

Time series of the horizontal and vertical length-scales are shown in Figure 3. These length-scales are calculated using the horizontal and vertical energy spectra as follows [5]:

$$l_h = \frac{2\pi \int_0^\infty E(k_h)\,\mathrm{d}k_h}{\int_0^\infty k_h E(k_h)\,\mathrm{d}k_h}, \qquad l_v = \frac{2\pi \int_0^\infty E(k_v)\,\mathrm{d}k_v}{\int_0^\infty k_v E(k_v)\,\mathrm{d}k_v}. \tag{31}$$

In the unstratified case, l_h decreases significantly over $0 \leq t \leq 10$. Increased stratification leads to a much smaller decrease (or even slight increase) in l_h, so the horizontal length-scale almost retains its original length. However, the vertical scale decreases significantly in all cases. For example, the $Fr_\ell = 0.32$ case retains its initial horizontal length-scale up to $t = 15$, at which time the vertical length-scale is about 30% of its initial value (see Figure 3b). After the onset of turbulence, the buoyancy Reynolds number decreases, and so the simulation transitions from marginally viscous (i.e. $Re_b \gtrsim 1$) to viscosity-affected (i.e. $Re_b \lesssim 1$) stratified turbulence. According to Figure 3a, the horizontal scales increase as Re_b decreases.

There are four interesting results in Figure 3: first of all, as seen in Figure 3c, using the Taylor hypothesis to estimate l_h can be a good approximation for the non-stratified case since l_h/L_h is almost constant (≈ 0.6) after the onset of turbulence. For stratified turbulence, on the other hand, $l_h/L_h \approx 0.4$ at the time of maximum ϵ_{tot} and increases with time. A similar trend for l_h for stratified turbulence has been observed in other experimental [37] and numerical [33] studies. Secondly, the vertical length-scales for $Fr_\ell = 0.64$ and $Fr_\ell = 0.32$ are shown in Figure 3d, scaled by the buoyancy scale $L_b = 2\pi u_{rms}/N$ (the factor 2π is included, following [16, 18], because it is the buoyancy wavenumber $k_b = N/u_{rms}$ that appears in applications, e.g. [2]). After turbulence commences (i.e. $t \gtrsim 20$), $l_v \sim L_b$ is a fairly good approximation. It is found that l_v is larger than L_b for the case with smaller Re_b, in agreement with the finding that l_v is set by viscosity at small Re_b [6, 35]. Moreover, Figures 3a and 3b also demonstrate an approximate equality of l_h and l_v for the non-stratified case. And finally, for the simulation with $Fr_\ell = 0.64$ and $Re_\ell = 800$, we can see an almost constant horizontal length-scale throughout the simulation (Figure 3a) and hence a fairly weak agreement with Taylor's hypothesis (Figure 3c). This behaviour is consistent with small Re_b in which the stratified flow seems to not be very turbulent.

4.2. *Effective eddy viscosity*

This section describes the results of directly measuring the effective eddy viscosity in the horizontal, vertical, and spherical directions. Effective eddy viscosity represents the effects of smaller-scale motions on eddies with wavenumbers below k_c. Four different cutoffs k_c have been employed in each of the horizontal, vertical,

and spherical directions to analyze the DNS results. The effective eddy viscosities have been averaged over a time range around the maximum dissipation rates (as in Figures 1c,d). Based on the Kraichnan eddy viscosity model [10], the effective cutoff k_c should be inside the inertial subrange. According to Figure 1d, $k_c = 80$ is inside the dissipation range. Therefore, we expect the measured eddy viscosity in this case to be small. All figures in this section are plotted in terms of $k^+ = k/k_c$ or $k_h^+ = k_h/k_c$ or $k_v^+ = k_v/k_c$. Moreover, the values of eddy viscosities in each figure (except Figure 8) have been normalized by the value of the corresponding molecular viscosity to show their effectiveness. The values of the SGS energy transfer in Figures 4c,d are normalized by those of the spherical SGS energy transfer at the test cutoff $k_c = 40$.

4.2.1. Stratification and effective eddy viscosity in different directions

First, we examine the $Fr_\ell = 0.64$ case when the cutoff wavenumber $k_c = 40$ is around the Ozmidov wavenumber $k_o \approx 35$. The unstratified case is also considered for comparison. Figure 4a,b show the non-stratified and stratified eddy viscosities, along with the Kraichnan theoretical eddy viscosity model [10]. The SGS energy transfer T_k^s, $T_k^{s,h}$, and $T_k^{s,v}$ are shown in Figures 4c,d. According to Figure 4a, the horizontal, vertical, and spherical eddy viscosities are very similar for non-stratified turbulence when $k^+ \gtrsim 0.1$. This behaviour is a sign of isotropic unstratified turbulence in which, for $k_c = 40$, the effective eddy viscosities are independent of direction. There are differences in the spherical, horizontal, and vertical eddy viscosities at large scales (i.e. $k^+ \lesssim 0.1$), which is to be expected given the anisotropy of the initial TG vortices. The slightly negative values of the effective eddy viscosity for small k^+ have also been previously reported [19, 20, 27, 38]. Large positive values of vertical eddy viscosity in Figure 4a when $k_v^+ \lesssim 0.1$ demonstrates a non-local energy transfer from large to small vertical scales (cf. $T_k^{s,v}$ in Figure 4c). It is important to note that for measuring the vertical eddy viscosity, we did not apply a restriction on the horizontal wavenumbers. Since the energy transfer in the non-stratified case is likely isotropic, the non-local energy transfer in the vertical direction may result from a local spherical transfer around k_c. The same conclusions hold for the large positive horizontal eddy viscosity as well.

In the stratified case, the horizontal eddy viscosity exhibits a very different behaviour: it has a positive plateau for $0.05 \lesssim k_h^+ \lesssim 0.8$ and a sharp cusp near k_c (Figure 4b). This behaviour is also clear in Figure 4d, in which for $0.05 \lesssim k_h^+ \lesssim 0.8$, the horizontal SGS energy transfer $T_k^{s,h}$ has an almost constant plateau, which has a value of 23% of the local horizontal SGS energy transfer at the cutoff k_c. However, ν_e is smaller overall than in the unstratified case. The presence of stratification results in a considerable difference between ν_e^h and ν_e^v: it increases the non-local energy transfer and effective eddy viscosity in the horizontal direction. A peak around $k_h^+ = 0.05$ is seen in the horizontal eddy viscosity, which is due to the effects of the initial conditions. Moreover, when $k_v^+ \lesssim 0.02$, the non-local vertical energy transfer is larger than the non-local horizontal energy transfer (Figure 4d). This behaviour suggests that there is a stronger energy transfer between large vertical scales and small vertical ones, which is consistent with the development of layers and small-scale turbulence with vertical wavenumbers above the cutoff k_c.

In summary, Figures 4b,d display two phenomena for $k^+ \ll 1$ in the stratified case. In the vertical, there is a transfer of energy from large to small scales. This large non-local energy transfer, which yields a large vertical eddy viscosity at small k_v, which is shown through the vertical eddy viscosity, is in agreement with the layering hypothesis of stratified turbulence (e.g. Billant & Chomaz [3]). The other phenomenon is the presence of a positive plateau for $0.05 \lesssim k_h^+ \lesssim 0.8$ in the

horizontal eddy viscosity and the horizontal SGS energy transfer $T_k^{s,h}$. Such non-local energy exchange between large and small horizontal scales is reminiscent of recent results in forced stratified turbulence [16] and the breakdown of columnar vortices [39, 40].

As mentioned above, the shape of the horizontal eddy viscosity in the stratified case shows a non-local energy transfer between large and small horizontal scales. All vertical scales are included in the calculation of $T_k^{s,h}$ and ν_e^h, so it is important to know if there is a specific vertical scale at which the non-local horizontal energy transfer occurs. In Figure 4b, it is clear that there is essentially no effective eddy viscosity in the spherical direction when $0.1 \leq k^+ \lesssim 0.8$. Similarly, there is no spherical SGS energy transfer for $0.1 \leq k^+ \lesssim 0.8$ (Figure 4d). There is no sign of non-local energy transfer between small and large k. As a result, the non-local horizontal energy transfer has to occur entirely at large vertical wavenumbers. This means that this non-local horizontal energy transfer and eddy viscosity correspond to a local energy transfer in the spherical direction.

We have shown that the non-local energy transfer in the horizontal direction occurs at vertical wavenumbers which are larger than k_c. Recent works [16, 39] have found non-local energy transfer between large-horizontal-scale motions and the buoyancy wavenumber $k_b = N/u_{rms}$. For $Fr_\ell = 0.64$ the maximum of N/u_{rms} for $15 \leq t \leq 20$ is about 6.5. If we normalize this value by using the test cutoff k_c in Figure 4, which is 40, it gives $k_b/k_c = 0.16$. By contrast, the Ozmidov wavenumber has $k_o/k_c \approx 1$. As seen in Figures 4b and d, there is a wide plateau in the horizontal direction for $0.05 \lesssim k_h^+ \lesssim 0.8$, which illustrates a non-local horizontal energy transfer between scales larger than the Ozmidov scale, including the buoyancy scale, and those smaller than the Ozmidov scale. It is noteworthy that the spherical SGS energy transfer in the stratified case is smaller than that of the non-stratified case at the cutoff $k_c = 40$, i.e. the local energy transfer, by a factor of around 2.

Consider the theoretical Kraichnan model, which is also shown in Figures 4a,b. This model has been calculated by assuming an infinite inertial subrange [20, 38] and is widely used [25, 41–43]. It has two distinct parts: a constant plateau for $k \ll k_c$ and a cusp near the cutoff k_c. By contrast, the effective eddy viscosity computed here is from DNS with a relatively short inertial subrange. Therefore, we do not expect to measure a plateau with the same amplitude as in Kraichnan's model. Batchelor et al. [32] applied a 'zero' plateau, while retaining the cusp parameters of the Kraichnan model, to LES of homogeneous turbulence generated by buoyancy. They found that this modification increases the accuracy of the mean-square velocity fluctuations in their simulations [32]. The long-dashed curve in Figure 4a shows the measured spherical eddy viscosity. Domaradzki et al. [19, 20] have measured the eddy viscosity for a case of non-stratified decaying turbulence; our measured unstratified spherical eddy viscosity is very similar to theirs.

4.2.2. Effects of different Reynolds numbers

Two simulations with the same initial Froude number $Fr_\ell = 0.64$ but with different initial Reynolds numbers $Re_\ell = 800$ and 6400 have been considered to show the effects of changing Reynolds numbers on the effective eddy viscosity. Since the Kolmogorov wavenumber for the lower Reynolds number case is $k_d = 42$, we have applied the test cutoff wavenumber $k_c = 20$ in both high and low-resolution cases to calculate the effective eddy viscosity.

Figure 5 shows the spherical and horizontal effective eddy viscosities normalized by their corresponding molecular viscosities in a,b; and normalized by just the molecular viscosity of case $Re_\ell = 6400$ in c,d. According to Figure 5a, the spherical eddy viscosity of case $Re_\ell = 800$ displays an almost zero plateau for $k \ll k_c$ and a

cusp near k_c. The effective eddy viscosity is much smaller than its corresponding molecular viscosity for $k, k_h < k_c$. In the $Re_\ell = 6400$ case, there is a more significant plateau, and the eddy viscosity in the cusp is much larger than its corresponding molecular viscosity (i.e. $\nu_e^+ > 1$). These two different behaviours can be explained by the critical role of the buoyancy Reynolds number if stratified turbulence is to be ensured. The maximum value of Re_b in the $Re_\ell = 800$ case is about 0.98 and the horizontal length-scale is almost constant versus time (Figure 3a), suggesting little if any stratified turbulence . Hence, the values of effective eddy viscosity are almost zero even at $k^+ \approx 0.7$.

The horizontal eddy viscosity for case $Re_\ell = 6400$ is dramatically affected by the occurrence of stratified turbulence. The shape of the eddy viscosity shows a large non-local horizontal eddy viscosity for $k_h \ll k_c$, and a sharp cusp nearby k_c (Figure 5b). The horizontal eddy viscosity for the case $Re_\ell = 800$ is correspondingly very weak and very similar to its spherical eddy viscosity. Figures 5c and d, illustrate the spherical and horizontal eddy viscosities in both cases which are normalized by the molecular viscosity of the case $Re_\ell = 6400$. It is found that increasing the Reynolds number increases the non-local horizontal eddy viscosity for $k_h \ll k_c$ and decreases the cusp value near k_c (Figures 5c,d).

4.2.3. Effects of different Froude numbers

In this section, we study the effects of various stratifications on the effective eddy viscosity when the initial Reynolds number is $Re_\ell = 6400$ and $k_c = 40$. Two cases – one with an initial Froude number of 0.64 and the other with one of 0.32 – have been considered. The horizontal eddy viscosity for case $Fr_\ell = 0.32$ is clearly larger than that of case $Fr_\ell = 0.64$ when $k_h^+ \lesssim 0.7$ (Figure 6b). In other words, there is an enhanced transfer of energy directly from large to small horizontal scales when the stratification is increased. The local energy transfer near the cutoff k_c, however, is less dependent on Fr_ℓ; the horizontal eddy viscosity of case $Fr_\ell = 0.64$ is slightly larger than that of case $Fr_\ell = 0.32$ at the cusp. By contrast, the effect of changing Fr_ℓ on the spherical and vertical eddy viscosities is relatively minor (Figures 6a,c).

4.2.4. Effects of changing the cutoff wavenumbers

To study the effects of the cutoff wavenumber k_c on the effective eddy viscosity, the case with $Re_\ell = 6400$ and $Fr_\ell = 0.64$ has been considered with four different cutoffs $k_c = 10,\ 20,\ 40,\ 80$ (Figure 7). As already mentioned, the Ozmidov wavenumber $k_o \approx 35$, so k_c ranges from smaller to larger than k_o.

Following Figure 7a towards 7d shows that by increasing the value of the test cutoff k_c, the horizontal eddy viscosity changes its shape by dramatically decreasing its non-local ($k_h \ll k_c$) and cusp ($k_h \approx k_c$) values. This trend means that by increasing the test cutoff k_c at fixed Re_ℓ, non-local and local horizontal eddy viscosity (energy exchange) decreases, with local energy transfer dominating non-local at large k_c. Similar behaviour was observed by Bartello et al. [21] in rotating stratified turbulence. When the cutoff k_c decreases toward the initial large scales, the horizontal eddy viscosity increases due to enhanced energy transfer between energetic horizontal motions and modes with $k_h > k_c$ (i.e. non-local horizontal energy transfer due to the elongated triads mechanism). However, when the cutoff k_c moves toward the dissipation range, modes with $k_h > k_c$ exchange less energy with energetic initial horizontal scales and more with modes with $k_h \lesssim k_c$ (i.e. the local triad mechanism). Therefore, local energy transfer dominates the non-local horizontal transfer for increased k_c [10, 21].

According to Figure 1d, $k_c = 80$ is in the dissipation range; thus, the measured eddy viscosities using this cutoff are on the order of the molecular viscosity or less. As seen in Figure 7d, at the cutoff point (i.e. $k^+ = 1$), the value of Kraichnan's

model is less than that of the molecular viscosity (i.e. $\nu_e^+ \lesssim 1$). This finding demonstrates that the cutoff value has been chosen inside the dissipation range in which the Kraichnan model is not valid. Furthermore, when $k^+ \gtrsim 0.1$, the horizontal, vertical, and spherical eddy viscosities of stratified turbulence overlap fairly well in Figure 7d, suggesting relative isotropy in the dissipation range in this case.

It is also interesting to consider the potential self-similarity of the effective eddy viscosity computed with different cutoffs k_c. Spherical, horizontal, and vertical effective eddy viscosities computed with four different test cutoff k_c are shown in Figure 8. For a better evaluation of self-similarity, the vertical axes are normalized [30, 38] by $[E(k_c)/k_c]^{1/2}$. Significant changes in the structure of the horizontal eddy viscosity (Figure 8b) demonstrate the absence of a self-similar inertial subrange when the cutoff k_c is applied in the horizontal direction. This non-similarity in the horizontal direction make sense because self-similarity is expected mainly when local energy transfer dominates (i.e. the similarity cascade [44]). By contrast, the vertical and spherical eddy viscosities show some degrees of self-similarity in the inertial subrange when $k^+, k_v^+ \gtrsim 0.1$ for $k_c \geq 20$, especially for $k_c \gtrsim k_o$ which is ≈ 35 (Figure 8a,c).

5. Conclusions

Decaying stratified and non-stratified turbulence has been analyzed to measure the spherical, horizontal, and vertical eddy viscosities in DNS results. As seen in previous studies, stratification decreases the total dissipation rate, and the time of peak dissipation is postponed. Furthermore, the energy spectrum steepens due to enhanced viscous effects when stratification increases or the Reynolds number decreases, due to the reduction of the buoyancy Reynolds number.

When $k_c = 40$, the spherical, horizontal, and vertical eddy viscosities overlap fairly well in the non-stratified case when $k^+ \gtrsim 0.1$ (i.e. small scales), but since the initial motions are anisotropic, there are clear differences between these eddy viscosities when $k^+ \lesssim 0.1$. In the non-stratified case, the non-local energy transfer in the horizontal or vertical directions may be interpreted as a local energy transfer in the spherical direction because of the Kolmogorov cascade. The effective eddy viscosities in stratified turbulence appear very different. When the cutoff is around the Ozmidov wavenumber, the horizontal and vertical eddy viscosities are quite different from one another. Furthermore, the horizontal SGS energy transfer $T_k^{s,h}$ at $k_h^+ \ll 1$ is around 20% of the local horizontal SGS energy transfer at $k^+ = 1$. Meanwhile, T_k^s at $k^+ = 1$ for the stratified case is two times smaller than that of the non-stratified case. These behaviours show an almost constant plateau in horizontal energy transfer for $k_h \ll k_c$, and a decrease in local energy transfer near k_c, in the presence of strong stratification. Positive values of the horizontal eddy viscosities demonstrate a forward energy cascade from large to small horizontal scales in stratified turbulence, as seen in other studies [4–7, 15–18].

These results are consistent with the findings of Augier et al. [39] in which a columnar vortex pair first transforms into layered structures at large horizontal scales. We claim that the large positive vertical eddy viscosity of stratified turbulence at large vertical scales (i.e. $k_v^+ \lesssim 0.02$) shows a non-local energy transfer from large to small vertical scales. Moreover, we have shown that for stratified turbulence, there is energy transfer directly from large to small horizontal scales in the range of large vertical wavenumbers, i.e. non-local in the horizontal direction but local in the spherical direction. This finding is reminiscent of the second stage of the vortex breakdown discussed by Augier et al. [39], in which

secondary Kelvin-Helmholtz instabilities are generated and ultimately transition into small-scale turbulence below the buoyancy scale. Our results show that energy may transfer directly to horizontal scales that are even smaller than the buoyancy scale. Further studies with a wider scale separation between the initial, buoyancy, and cutoff wavenumbers are needed to investigate the details of direct non-local horizontal energy transfer between the (large) energetic scales with wavenumbers below k_c, and small-scale motions with wavenumbers above k_c. However, this large separation would requires a high Re_ℓ and Re_b.

Changing the cutoff wavenumber k_c has a considerable effect on the shapes and values of effective eddy viscosities. When the cutoff is near the scale of the initial conditions, the values of measured horizontal eddy viscosity shows a non-local transfer for $k_h \ll k_c$. However, by moving the cutoff k_c towards the Kolmogorov scale, the effective eddy viscosity decreases dramatically. This behaviour demonstrates a decrease in the non-local horizontal energy transfer by increasing the value of test cutoff k_c into the dissipation range, as expected.

We have confirmed that stratification modifies the effective eddy viscosity qualitatively. A stratified inertial subrange that clearly includes scales above and below the Ozmidov scale requires very high Reynolds number. Such an inertial subrange is difficult to obtain with a DNS approach. By contrast, LES of stratified turbulence, in which the Ozmidov scale is not resolved, is seriously affected by anisotropic features. Kraichnan's [10] theoretical model is based on the assumption that local energy transfer, near the cutoff k_c, dominates non-local energy transfer, at $k \ll k_c$. This idea was also confirmed by Domaradzki et al. [20] in DNS results of non-stratified isotropic turbulence. However, as shown here, the presence of stratification increases the non-local horizontal energy transfer for $k_h \ll k_c$, between large energetic and SGS horizontal motions, which is significant. Therefore, an isotropic SGS model such as the Kraichnan model (with the infinite inertial subrange) does not seem to be a proper approach for LES of stratified turbulence. For example, in a recent paper by Schaefer-Rolffs and Becker [45] about large-scale atmospheric dynamics, where stratification is important, a dynamic Smagorinsky model has been applied just to the horizontal direction. Our future work will include investigations on how to improve current SGS models to consider the effects of anisotropy and non-locality and hence the effects of stratification in the horizontal direction.

6. Acknowledgment

The authors would like to thank Kevin Lamb and two anonymous referees for helpful discussions and comments on this paper. This work was made possible by the facilities of the Shared Hierarchical Academic Research Computing Network (SHARCNET: www.sharcnet.ca) and Compute/Calcul Canada. Financial support from the Natural Sciences and Engineering Research Council of Canada is gratefully acknowledged.

References

[1] J. J. Riley, and M.-P. Lelong, *Fluid motions in the presence of strong stable stratification*, Annu. Rev. Fluid Mech. 32 (2000), pp. 613-657.
[2] P. Billant, and J.-M. Chomaz, *Experimental evidence for a new instability of a vertical columnar vortex pair in a strongly stratified fluid*, J. Fluid Mech. 418 (2000), pp. 167-188.
[3] P. Billant, and J.-M. Chomaz, *Self-similarity of strongly stratified inviscid flows*, Phys. Fluids 13 (2001), pp. 1645-1651.
[4] J. J. Riley, and S. M. de Bruyn Kops, *Dynamics of turbulence strongly influenced by buoyancy*, Phys. Fluids 15 (2003), pp. 2047-2059.

[5] E. Lindborg, *The energy cascade in strongly stratified fluid*, J. Fluid Mech. 550 (2006), pp. 207-242.
[6] G. Brethouwer, P. Billant, E. Lindborg, and J.-M. Chomaz, *Scaling analysis and simulation of strongly stratified turbulent flows*, J. Fluid Mech. 585 (2007), pp. 343-368.
[7] J. J. Riley, and E. Lindborg, *Stratified turbulence: a possible interpretation of some geophysical turbulence measurements*, J. Atmos. Sci. 65 (2008), pp. 2416-2424.
[8] J. L. Lumley, *The spectrum of nearly inertial turbulence in stably stratified fluid*, J. Atmos. Sci. 21 (1964), pp. 99-102.
[9] J. Smagorinsky, *General circulation experiments with the primitive equations. I. The basic experiment*, Mon. Weather Rev. 94 (1963), pp. 99-164.
[10] R. H. Kraichnan, *Eddy viscosity in two and three dimensions*, J. Atmos. Sci. 33 (1976), pp. 1521-1536.
[11] J.-P. Chollet, and M. Lesieur, *Parametrization of small scales of three-dimensional isotropic turbulence utilizing spectral closures*, J. Atmos. Sci. 38 (1981), pp. 2747-2757.
[12] D. A. Siegel, and J. A. Domaradzki, *Large-eddy simulation of decaying stably stratified turbulence*, J. Phys. Oceanogr. 24 (1994), pp. 2353-2386.
[13] M. Lesieur, and O. Métais, *New trends in large-eddy simulations of turbulence*, Annu. Rev. Fluid Mech. 28 (1996), pp. 45-82.
[14] A. N. Kolmogorov, *The local structure of turbulence in incompressible viscous fluid for very large Reynolds number*, Dok. Akad. Nauk. SSSR 30 (1941), pp. 301-305.
[15] M. L. Waite, and P. Bartello, *Stratified turbulence dominated by vortical motion*, J. Fluid Mech. 517 (2004), pp. 281-308.
[16] M. L. Waite, *Stratified turbulence at the buoyancy scale*, Phys. Fluids A 23 (2011), 066602.
[17] S. Almalkie, and S. M. de Bruyn Kops, *Kinetic energy dynamics in forced, homogeneous, and axisymmetric stably stratified turbulence*, J. Turbul. 13 (2012), pp. 1-32.
[18] M. L. Waite, *Direct numerical simulations of laboratory-scale stratified turbulence*, Modelling Atmospheric and Oceanic Flows: Insights from Laboratory Experiments, T. von Larcher and P. Williams (eds.), American Geophysical Union (2013), in press.
[19] J. A. Domaradzki, R. W. Metcalfe, R. S. Rogallo, and J. J. Riley, *Analysis of subgrid-scale eddy viscosity with use of results from direct numerical simulations*, Phys. Rev. Lett. 58 (1987), pp. 547-550.
[20] A. J. Domaradzki, W. Liu, and M. E. Brachet, *An analysis of subgrid-scale interactions in numerically simulated isotropic turbulence*, Phys. Fluids A 5 (1993), pp. 1747-1759.
[21] P. Bartello, O. Métais, and M. Lesieur, *Geostrophic versus wave eddy viscosities in atmospheric models*, J. Atmos. Sci. 53 (1996), pp. 564-571.
[22] K. S. Gage, *Evidence for a $k^{-5/3}$ law inertial range in mesoscale two-dimensional turbulence*, J. Atmos. Sci. 36 (1979), pp. 1950-1954.
[23] D. K. Lilly, *Stratified turbulence and the mesoscale variability of the atmosphere*, J. Atmos. Sci. 40 (1983), pp. 749-761.
[24] H.-J. Kaltenbach, T. Gerz, and U. Schumann, *Large-eddy simulation of homogeneous turbulence and diffusion in stably stratified shear flow*, J. Fluid Mech. 280 (1994), pp. 1-40.
[25] G. F. Carnevale, M. Briscolini, and P. Orlandi, *Buoyancy- to inertial-range transition in forced stratified turbulence*, J. Fluid Mech. 427 (2001), pp. 2205-239.
[26] S. Remmler, and S. Hickel, *Direct and large eddy simulation of stratified turbulence*, Inter. J. of Heat and Fluid Flow 35 (2012), pp. 13-24.
[27] A. J. Domaradzki, and S. Radhakrishnan, *Effective eddy viscosities in implicit modelling of decaying high Reynolds number turbulence with and without rotation*, Fluid Dynamics Research 36 (2005), pp. 385-406.
[28] P. Moin, and K. Mahesh, *Direct numerical simulation: A tool in turbulence research*, Annu. Rev. Fluid Mech. 30 (1998), pp. 539-578.
[29] H. A. Rose, and P. L. Sulem, *Fully developed turbulence and statistical mechanics*, Le Journal de Physique 39 (1978), pp. 441-484.
[30] S. B. Pope, *Turbulent Flows*, Cambridge University Press, Cambridge (2000).
[31] M. Lesieur, *Turbulence in Fluids*, Kluwer Acad. Publrs., Dordrecht (1990).
[32] G. K. Batchelor, V. M. Canuto, and J. R. Chasnov, *Homogeneous buoyancy-generated turbulence*, J. Fluid Mech. 235 (1992), pp. 349-378.
[33] D. A. Hebert, and S. M. de Bruyn Kops, *Predicting turbulence in flows with strong stable stratification*, Phys. Fluids 18 (2006), 066602.
[34] D. R. Durran, *Numerical methods for fluid dynamics with application to geophysics*, Springer, New York (2010).
[35] D. A. Hebert, and S. M. de Bruyn Kops, *Relationship between vertical shear rate and kinetic energy dissipation rate in stably stratified flows*, Geophys. Research Lett. 33 (2006), L06602.
[36] P. Bartello, and S. M. Tobias, *Sensitivity of stratified turbulence to the buoyancy Reynolds number*, J. Fluid Mech. 725 (2013), pp. 1-22.
[37] O. Praud, A. M. Fincham, and J. Sommeria, *Decaying grid turbulence in a strongly stratified fluid*, J. Fluid Mech. 522 (2005), pp. 1-33.
[38] O. Métais, and M. Lesieur, *Spectral large-eddy simulation of isotropic and stably stratified turbulence*, J. Fluid Mech. 239 (1992), pp. 157-194.
[39] P. Augier, J.-M. Chomaz, and P. Billant, *Spectral analysis of the transition to turbulence from a dipole in stratified fluid*, J. Fluid Mech. 713 (2012), pp. 86-108.
[40] A. Deloncle, P. Billant, and J.-M. Chomaz, *Nonlinear evolution of the zigzag instability in stratified fluids: a shortcut on the route to dissipation*, J. Fluid Mech. 599 (2008), pp. 229-239.
[41] M. Lesieur, and R. Rogallo, *Large-eddy simulation of passive scalar diffusion in isotropic turbulence*, Phys. Fluids A 1 (1989), pp. 718-722.
[42] S. Cerutti, C. Meneveau, and O. M. Knio, *Spectral and hyper viscosity in high-Reynolds-number turbulence*, J. Fluid Mech. 421 (2000), pp. 307-338.
[43] M. Briscolini, and P. Santangelo, *The non-Gaussian statistics of the velocity field in low-resolution*

large-eddy simulations of homogeneous turbulence, J. Fluid Mech. 270 (1994), pp. 199-218.
[44] R. H. Kraichnan, *Inertial ranges in two-dimensional turbulence*, Phys. Fluids 10 (1967), pp. 1417-1423.
[45] U. Schaefer-Rolffs, and E. Becker, *Horizontal momentum diffusion in GCMs using the dynamic Smagorinsky model*, Mon. Wea. Rev. 141 (2013), pp. 887-899.

Table 1. List of numerical simulations for DNS.

Identifier	Fr_ℓ	Re_ℓ	n	k_{max}/k_d
$F0.6$	0.64	6400	768	$0.73 - 0.94$
$F0.3$	0.32	6400	768	$0.69 - 0.84$
UNST	∞	6400	768	$0.5 - 1.25$
$F0.6R$	0.64	800	256	$1.21 - 1.41$
k_c	10	20	40	80

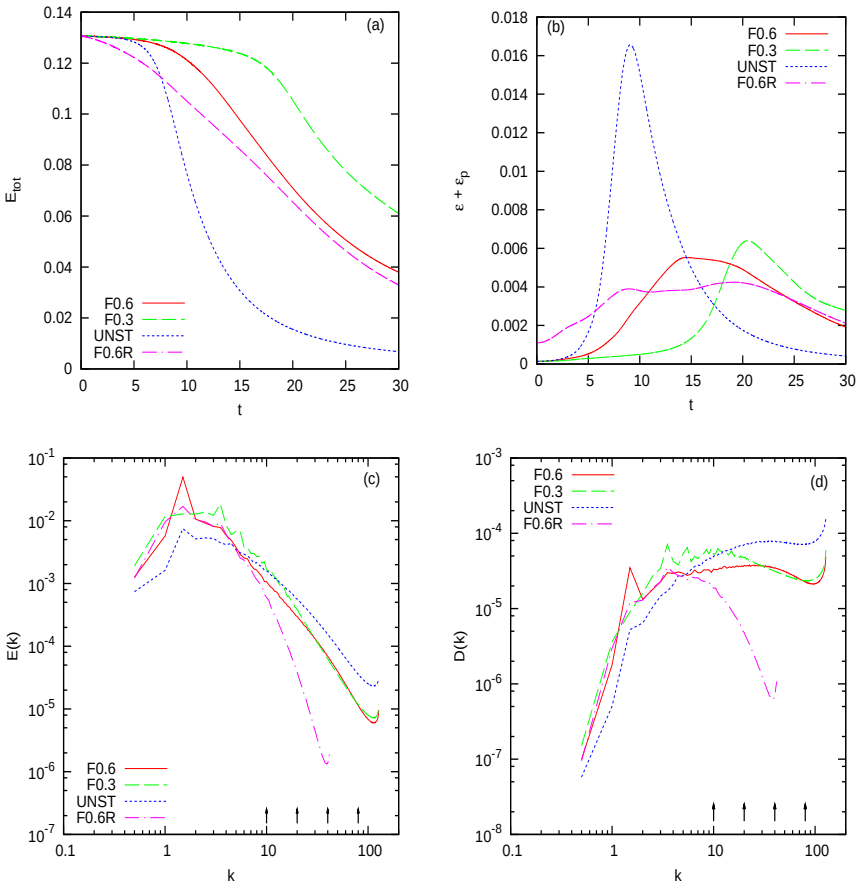

Figure 1. (a) Total energy, (b) total dissipation rate, (c) time-averaged kinetic energy spectra, and (d) time-averaged dissipation spectra. Arrows indicate values of the different test cutoffs k_c, which are presented in Section 4.2.

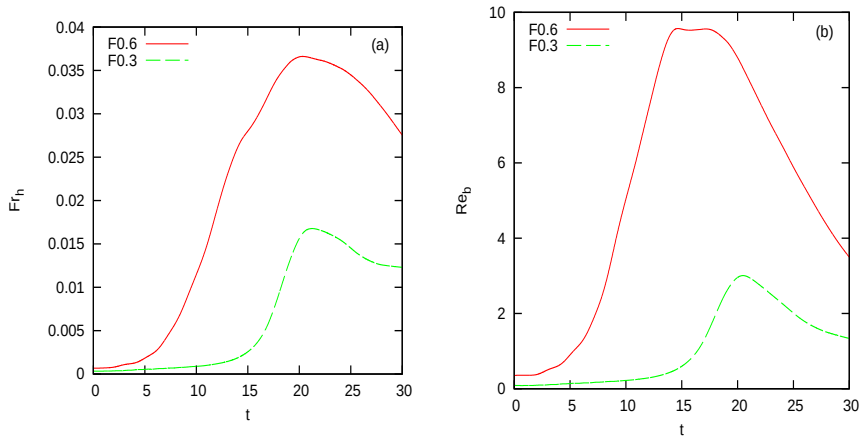

Figure 2. Time series of (a) horizontal Froude number and (b) buoyancy Reynolds number for the two stratified simulations with $Re_\ell = 6400$. Froude and buoyancy Reynolds numbers are computed with a horizontal length scale obtained from Taylor's hypothesis, which may not be valid at early times.

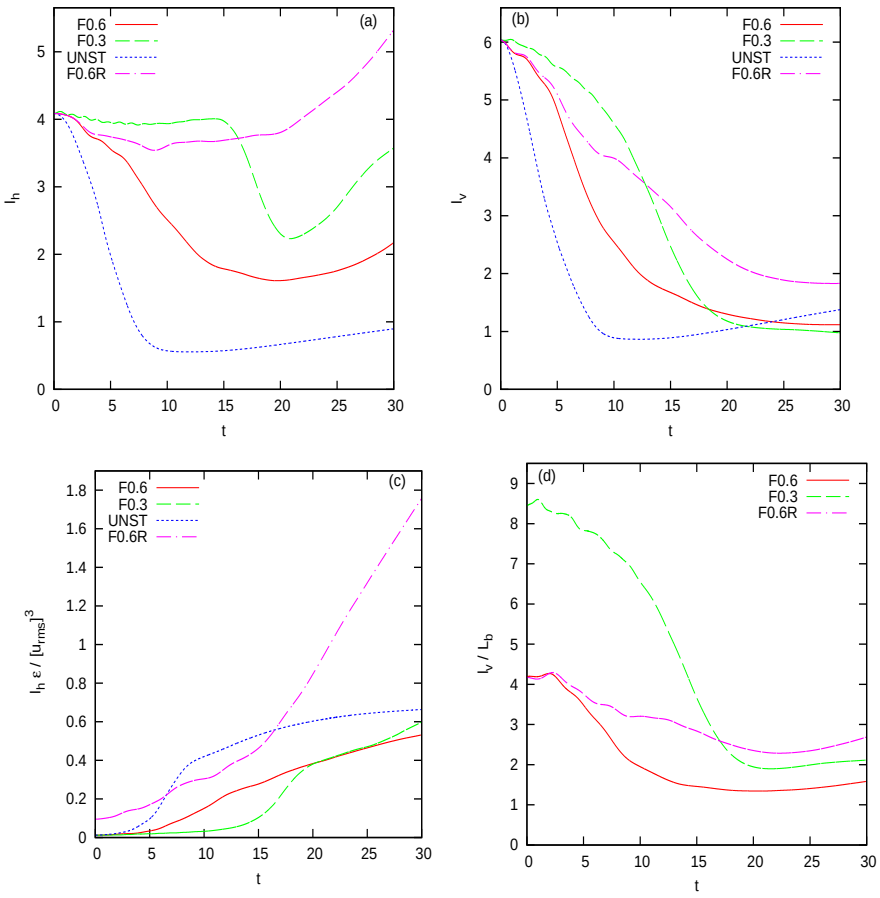

Figure 3. Time series of (a) the horizontal length-scale, (b) the vertical length-scale, (c) the horizontal length-scale scaled using the Taylor hypothesis, and (d) the vertical length-scale scaled by the buoyancy scale L_b.

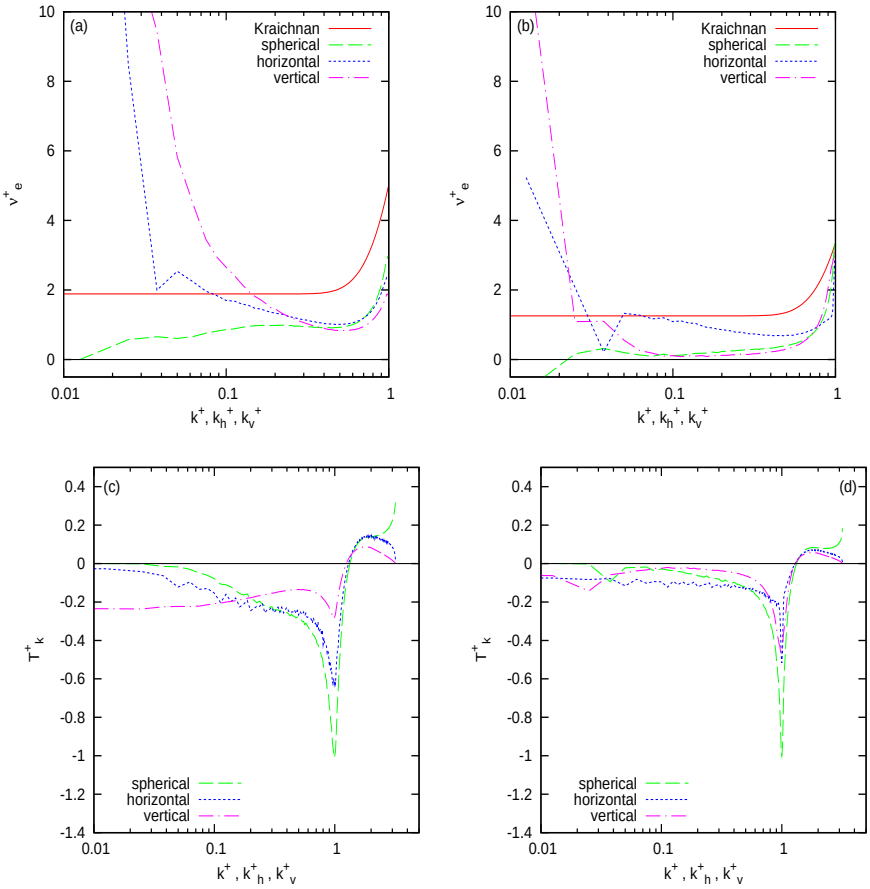

Figure 4. Effective eddy viscosity for (a) the unstratified case and (b) corresponding stratified case (runs UNST and $F0.6$, respectively), with $k_c = 40$. Based on the time average over the maximum dissipation rates. The theoretical eddy viscosity for the Kraichnan [41] model gives by the solid line. Here, ν_e^+ stands for ν_e/ν, ν_e^h/ν, and ν_e^v/ν; and $k^+ = k/k_c$, $k_h^+ = k_h/k_c$, $k_v^+ = k_v/k_c$ in all cases. Panels (c) and (d) show the corresponding SGS energy transfer spectra for the unstratified and stratified cases, respectively. Values in (c) and (d) are normalized by the corresponding absolute values of $T_k^s(k_c)$ for the non-stratified and stratified cases. The solid black line indicates the value of zero.

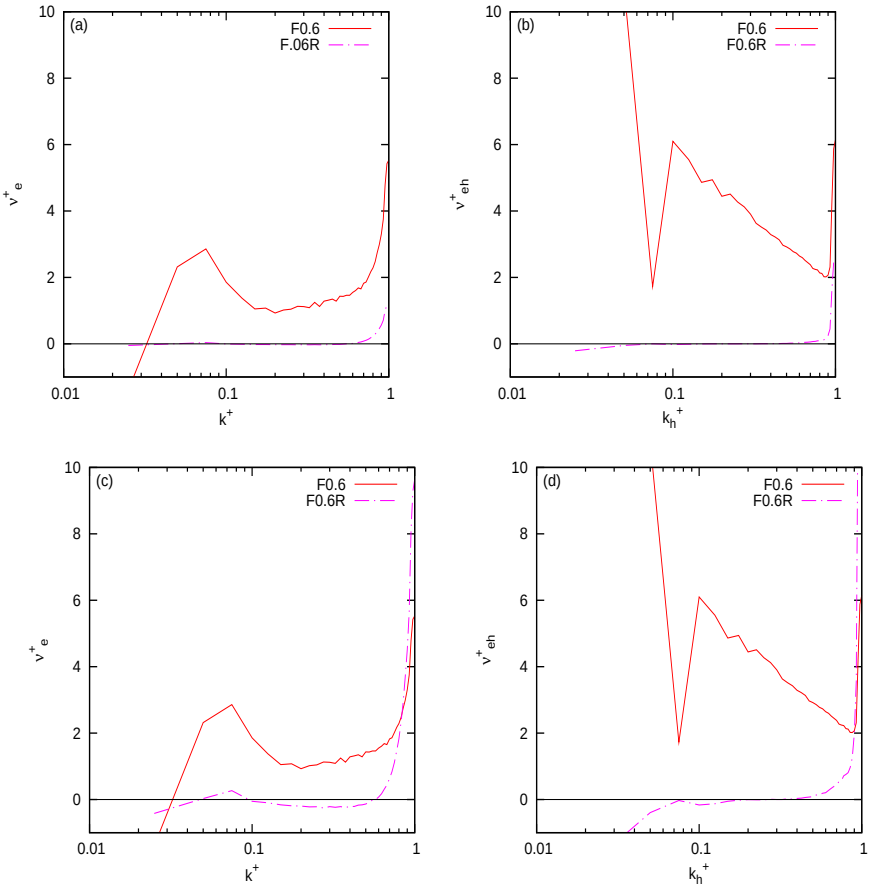

Figure 5. Effective (a,c) spherical and (b,d) horizontal eddy viscosity for two simulations with $Fr_\ell = 0.64$ and $Re_\ell = 6400$ (solid) and 800 (dashed), with $k_c = 20$. In (a,b), the eddy viscosity of each case are normalized by the corresponding molecular viscosity; in (c,d) they are normalized by the $Re_\ell = 6400$ molecular viscosity. The solid black line indicates the value of zero.

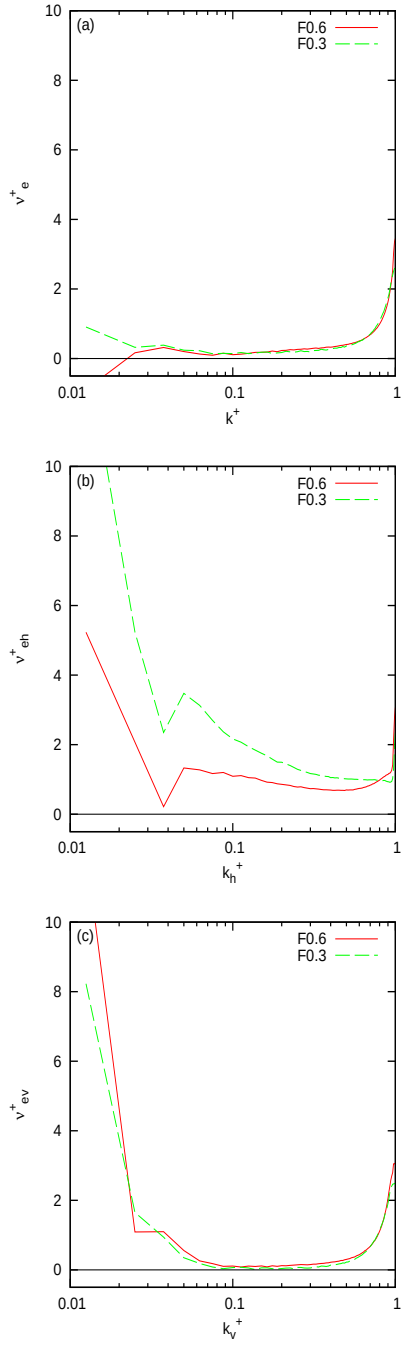

Figure 6. (a) Spherical, (b) horizontal, and (c) vertical effective eddy viscosity for different stratification (runs $F0.6$ and $F0.3$) at $k_c = 40$. The solid black line indicates the value of zero.

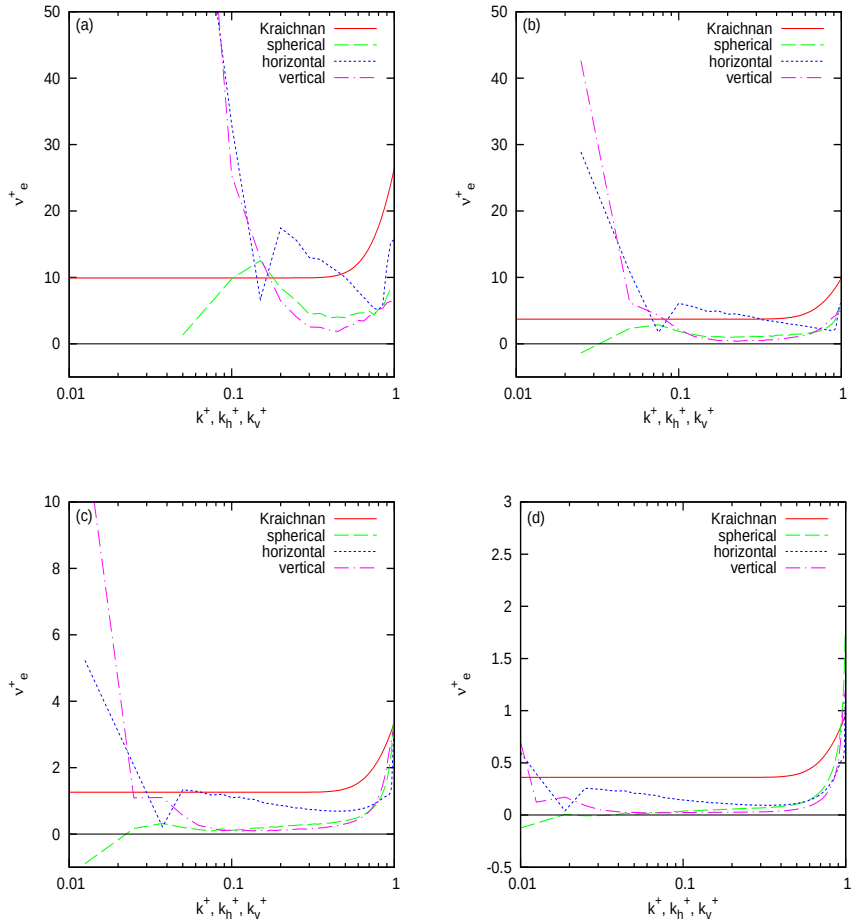

Figure 7. Effective eddy viscosities $F0.6$ computed with different cutoff wavenumber k_c = (a) 10, (b) 20, (c) 40, and (d) 80. The solid red line: the Kraichnan [41] model. The scales of the vertical axes varies in panels (c) and (d) from (a,b). The solid black line indicates the value of zero.

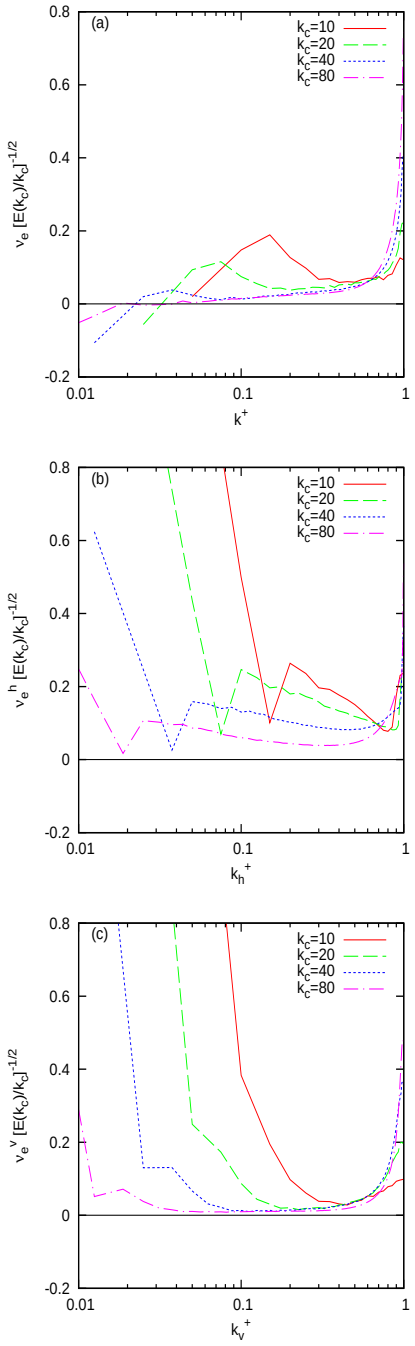

Figure 8. (a) Spherical, (b) horizontal, and (c) vertical effective eddy viscosity $F0.6$ using different cutoff wavenumbers k_c. Eddy viscosities are normalized [30, 38] by $[E(k_c)/k_c]^{1/2}$ to evaluate the self-similarity clearly. The solid black line indicates the value of zero.